SURFACE ROCK CONTROLS ON THE DEVELOPMENT OF DESERT VARNISH IN THE MOJAVE DESERT

By

Eric James Zautner

Submitted to the graduate degree program in Geography and Atmospheric Science and the Graduate Faculty of the University of Kansas in partial fulfillment of the requirements for the degree of Master of Science.

_____
Chairperson Daniel R. Hirmas, Ph.D.

_____
William C. Johnson, Ph.D.

_____
Xingong Li, Ph.D.

Date Defended: 7/22/2016

The Thesis Committee for Eric James Zautner

certifies that this is the approved version of the following thesis:

SURFACE ROCK CONTROLS ON THE DEVELOPMENT OF DESERT VARNISH IN THE MOJAVE DESERT

_____

Chairperson Daniel R. Hirmas, Ph.D.

Date Approved: 7/22/2016

ABSTRACT

Desert varnish is a commonly occurring feature on surface rocks of stable landforms in arid regions. The objectives of this study were to investigate how desert varnish is related to the properties of the rocks on which it forms and how varnish is related to landform surface age and stability. To accomplish these objectives, approximately 350 varnished rocks from previously dated sites in the Mojave Desert were collected, photographed, converted to 3-D models, and analyzed to determine the extent, intensity, and patterns of desert varnish and how the desert varnish was related to land surface age and stability. Our results show a link between increasingly stronger varnish expression and both landform age and stability. We found a potential interaction between vesicular (V) horizons and the formation of the rubified ventral varnish. The rocks in this study showed a maximum varnish expression at a depth below the embedding plane that corresponded to the depth of V horizons when present and the lowest portion of the rock when absent. When V horizons were present, the varnish tended to be strongest near the lower boundary of these horizons. This interaction between the V horizons and location of maximum varnish expression on the rock may be due to the effect of V horizons on infiltration and the retention of water at those depths. The relationship between ventral rubification, rock size, and age shown in this study suggest that stable land surface environments (i.e., stable landforms and large surface rocks) create conditions needed for strongly expressed varnish. In the absence of traditional dating techniques, these relationships could be used to estimate the ages of Mojave Desert landforms.

ACKNOWLEDGEMENTS

I would like to thank Dr. Daniel Hirmas for encouraging me to attend graduate school as his student and always showing me the way forward throughout my time at the University of Kansas. I am also thankful for the assistance of Drs. William Johnson and Xingong Li for assisting me as part of my thesis committee. My research would not have been possible without the computer programming skills of Dr. James Miller and the diligent fieldwork of fellow graduate student Kim Drager. The photography aspect of the project was aided by the resources of Dr. Steven Hasiotis and the experimental design of Michael Wu. Fieldwork was made possible by a research permit from the Mojave National Preserve and the National Park Service. I would finally like to express appreciation to my family for believing that I could accomplish this task and make them proud.

TABLE OF CONTENTS

CHAPTER 1. INTRODUCTION

Rock coatings accumulate where rock surfaces are stable enough to accrete clay minerals through geochemical, biological, or physical processes (Dorn, 2009a; 2009b). One of these coatings known as 'rock varnish' occurs in arid and semi-arid regions and is composed of about 70% clay minerals, the remainder of which is composed of iron- and manganese-oxides and hydroxides, detrital silica, and calcium carbonate (Dorn and Oberlander, 1982). Rock varnish is distinguished by a black (melanized) color on the exposed dorsal surface and an orange (rubified) color on the embedded ventral surface. The orange varnish on the ventral side contains more iron (~10% FeO_2 and ~3% MnO_2 by weight) and the black varnish on the dorsal side contains more manganese (~20% MnO_2 by weight) (Potter and Rossman, 1977, Perry and Adams, 1978). Since this is primarily a time-dependent process, the accumulation of desert rock varnish can be used to approximate the age and stability of surficial deposits and geomorphic surfaces (Birkeland, 1984; Colman et al., 1987).

The intensity and extent of rock varnish has been used as a relative age indicator in previous work (McFadden et al., 1989). On alluvial fans in Death Valley, California, varnish microlaminations (VML) showed that rock varnish could reveal more detailed information about pavement disturbance than traditional ^{14}C dating (Liu and Dorn, 1996). Considerable doubt regarding the validity of varnish techniques (Dorn, 1998; Beck et al., 1998), however, temporarily stifled rock varnish research although investigations in the field appear to have rebounded recently. For example, in the Cima Volcanic Field, California, Liu (2003) showed that radiometrically calibrated varnish microstratigraphy could be used to estimate surface exposure ages.

Surface rocks protect sediments and soil from removal by wind and water while contributing to the stability of landforms (Cooke et al., 1993). Rock-mantled slopes can decrease sediment transport rates if rocks occupy more than 70% of the land surface area since they protect underlying fines and provide resistance to flow. By contrast, land surfaces that are sparsely mantled with rocks can enhance the transport rate by concentrating flow (Poesen and Lavee, 1991). In a study on steep desert slopes abutting rapid suburban development in the Phoenix, Arizona, metropolitan area, Liu (2008) suggested that mass wasting on these landforms occurred throughout the Holocene, with landslide events as little as 300 years ago. Since rock varnish develops upon exposure at the land surface, rocks displaying iron varnish on their dorsal sides could be an indication of instability.

Land surface stability can be related to climate change, landscape dynamics, and paleo-reconstruction. By studying differing alluvial fan shape and formation processes on sites dated at the Pleistocene-Holocene transition, Harvey and Wells (2003) showed that fan processes are controlled by water and sediment supply from hillslopes, which is ultimately controlled by shifts in climate. It has been suggested that temporal relationships between alluvial fan deposition and climate variations could be extrapolated across a region (McDonald, et al., 2003). In the Negev Desert, Israel – a region less prone to climate variation than the Mojave Desert – the combination of long-term aridity, lack of vegetation and bioturbation, and rapid accumulation of desert pavement can be indicative of ancient and stable landscapes (Matmon et al., 2009).

Helms et al. (2003) field-tested a technique at Pilot Knob, California, specifically developed to semi-quantify rock varnish using Munsell color notation. In this study, weighted chromas, values, and hues were determined and plotted on a Munsell color wheel. While providing a foundation for future work, Helms et al. (2003) did not directly exam the relationship

between dorsal (exposed) and ventral (embedded) surfaces of rocks and their relation to landscape age and stability.

The goals of this work were to (1) investigate the relationship of varnish expression on both dorsal and ventral sides of the rock to rock properties such as size, surface roughness, and lithology and (2) to examine the relationship between landform age and varnish expression. At sites where absolute dating techniques have limitations or are impractical, an increased understanding of varnish development on both ventral and dorsal surfaces of rocks will allow for a more complete evaluation of surface ages across a landscape.

CHAPTER 2. MATERIALS AND METHODS

Site Selection

Samples were collected in a portion of the Mojave Desert located within San Bernardino County, California (Fig. 1). Three key factors were considered during the site selection process: (1) the presence of desert pavement, (2) an established landform chronology, and (3) the accessibility of precise locations documented in previous studies. Additionally, we sought to investigate varnish formation within both volcanic and alluvial settings, and, thus, sites were chosen that represented both of these geomorphic environments (Table 1).

Eight sites were chosen across three study areas representing alluvial landforms (Tables 1 and 2): the Providence Mountains (McDonald et al., 2003), Kingston Wash (Mahan et al., 2007), and the southern Fry Mountains (Hirmas and Graham, 2011). Nine volcanic study sites were chosen (Table 2); seven were located in the Cima Volcanic Field (Wells et al., 1995) and the remaining were located on the flanks of Pisgah and Amboy Craters (Phillips, 2003).

Field Sampling

In order to maintain consistency and eliminate bias in the sampling methods, the following procedure was used. At each site, two perpendicular 10-m transects were marked down slope and across slope using measuring tapes within approximately 10 m of the previously determined location in the literature (Table 1) using a handheld GPS unit. At three of the sites, individual transects were lengthened or shortened to accommodate the geometry of the landform surface. Slope grade, aspect, and shape were measured using a clinometer and compass. Four 5-m sections of the measuring tapes extended from the center of the perpendicular transects and

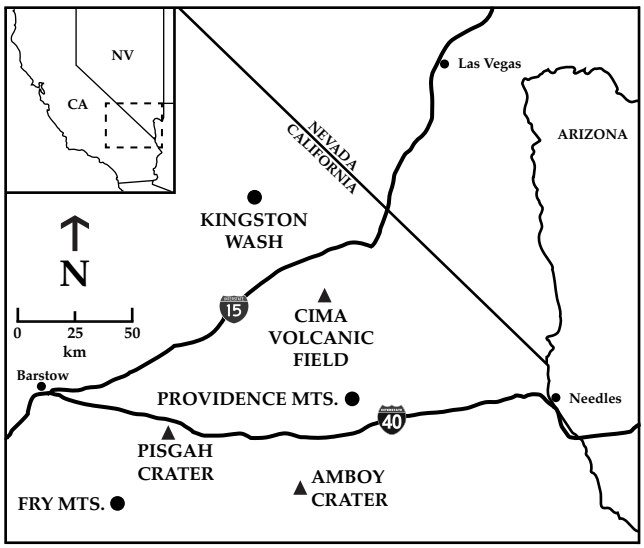

Fig. 1. The six areas within the Mojave Desert sampled in this study where landform ages were previously determined. Circles show alluvial locations and triangles represent volcanic locations.

Table 1
Ages and characteristics of sites selected for this study.

Elevation (m)	Previous dating techniques(s)[a]	No. of sites	Ages (ka)	Material dated	Lithology	Landform
Amboy Crater (Phillips, 2003)						
~235	^{36}Cl	1	79.4	volcanic flows	basalt	volcanic cones, flows
Cima Volcanic Field (Phillips, 2003)						
~800-1100	^{36}Cl	7	13-85	pavement, scoria, flow surface	basalt, scoria	volcanic cones, flows
Fry Mountains (Hirmas and Graham, 2011)						
~885	OSL	2	2-6	alluvial deposits	granite to quartz monzonite; biotite diorite[b]	alluvial fans
Kingston Wash (Mahan et al., 2007)						
~470	OSL	3	18-52	alluvial deposits	granite porphyry[c]	alluvial plain
Pisgah Crater (Phillips, 2003)						
~765	^{36}Cl	1	22.5	volcanic flows	basalt	volcanic cones, flows
Providence Mountains (McDonald et al., 2003)						
~800-900	^{14}C, IRSL, SS	3	28-1070	alluvial deposits	felsic plutonic; including granite and granodiorite[d]	alluvial fans

[a] ^{36}Cl = cosmogenic nuclide (^{36}Cl), OSL = optically stimulated luminescence, ^{14}C = radiocarbon, IRSL = infrared stimulated luminescence, SS = estimated from soil stratigraphy.

[b] Lithology determined from Dibblee (1967).

[c] Lithology determined from Calzia et al. (1987).

[d] Lithology determined from Bedford et al. (2006).

Table 2
Landform data for indivdual study sites grouped by study area.

Study sites	Latitude (°)	Longitude (°)	Slope (%)	Slope shape (up/across)	Aspect	Roughness
Amboy Crater						
VA1	34.54655	115.79653	7	linear/linear	190° S	2.57±1.37
Cima Volcanic Field						
VC1	35.21654	115.75151	10	concave/linear	300° W	5.00±3.99
VC2	35.19494	115.82752	2	linear/linear	117° E	7.02±1.34
VC3	35.18187	115.82227	6	concave/convex	30° N	6.72±2.85
VC4	35.20785	115.79301	5	linear/linear	121° E	7.15±0.78
VC5	35.19964	115.83381	2	linear/linear	250° SW	4.94±1.33
VC6	35.48105	115.84111	14	convex/linear	25° N	4.45±2.13
VC7	35.17933	115.81753	15	convex/linear	48° NE	7.71±1.49
Fry Mountains						
Pa1	34.46361	116.70187	6	linear/linear	275° W	2.26±1.14
Pai1	34.4716	116.70807	5	convex/convex	289° SW	5.79±2.13
Kingston Wash						
AK1	35.6244	116.0497	5	linear/linear	230° SW	1.76±0.74
AK1	35.62466	116.05077	4	linear/linear	238° SW	2.14±0.63
AK1	35.62439	116.04233	8	linear/linear	334° NW	1.39±0.48
Pisgah Crater						
VP1	34.75591	116.37663	4	convex/convex	166° S	6.98±2.89
Providence Mountains						
AP1	34.88116	115.63482	9	linear/linear	280° W	2.19±1.56
AP2	34.90446	115.61364	8	linear/linear	242° W	1.82±1.37
AP3	34.89926	115.63646	4	linear/linear	250° W	2.76±0.79

Values following a ± symbol correspond to 1 standard deviation.

were labeled D1 through D4 in clockwise fashion, beginning with the upslope orientated transect (Fig. 2).

The desert pavement immediately adjacent to each transect section (i.e., D1, D2, D3, D4) was digitally photographed in 1-m intervals (T2i DSLR, 18-55mm f/3.5-5.6, Canon, Tokyo, Japan) from a height of about 1 m directly above the land surface. Additional photographs were taken from the center of the transect facing out to the horizon along the four cardinal directions. Vesicular (V) horizons (if present) were described at the end of each of the four transect sections following Schoeneberger et al. (2012).

Rocks were categorized by size into 3 classes using the semi-major axis length of each rock. Small rocks had a diameter of 5-10 cm, medium rocks ranged from 10-20 cm, and large rocks exceeded 20 cm. Ten medium rocks and ten small rocks were taken from each site, with the exception of two alluvial sites due to the lack of medium sized rocks. In addition, five large rocks with semi-major axis lengths of roughly 20-50 cm were taken from each alluvial site; no large rocks were observed at any of the volcanic sites. Rocks that overlapped any of the four transects were eligible for collection. The closest rock of small or medium size class to the transect center was selected and the process continued outward until 10 medium and 10 small rocks were collected (Fig. 2). At the alluvial sites, 5 large rocks were selected from within or immediately adjacent to the transect. Small horizontal lines were marked at 3 locations on each rock with a white paint pen to indicate where the rock had been embedded in the surface along with arrows to indicate the vertical orientation of the rock. After drying, each rock was placed in a gallon plastic bag along with an identification number containing the site name, size class, and distance from the center of the transect where it was collected.

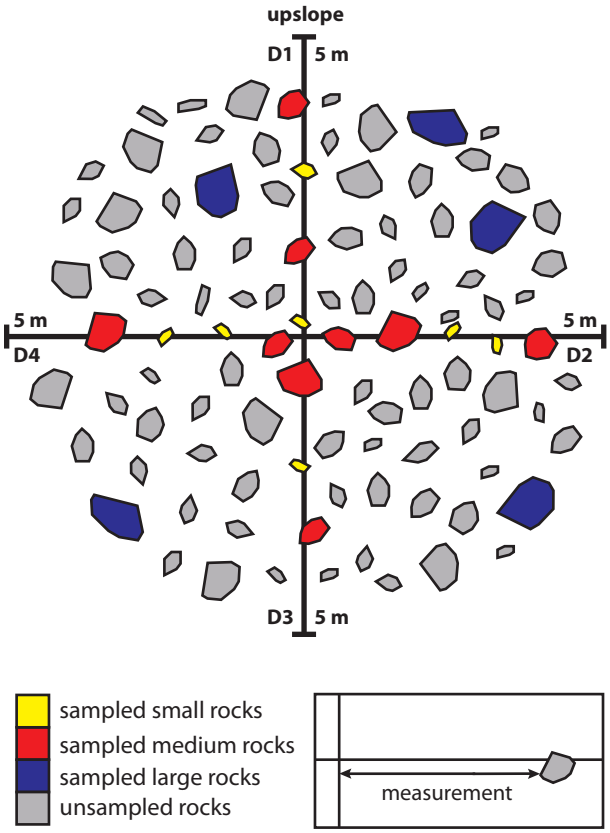

Fig. 2. Two crossing 10-m transects were set up at each site and rocks were collected. Small and medium rocks with major axes of 5–10 and 10–20 cm, respectively, closest to the point where the two transects crossed were collected if they overlapped either transect. In addition, 5 large rocks with major axes >20 cm were collected from the immediate area if present.

Digital 3-D Mapping

The rocks were gently washed, allowed to dry, and weighed. A photography backdrop was set up with lighting from 10 angles to minimize shadows and the variability of lighting conditions between shooting sessions (Fig. 3). A DSLR camera (Canon T2i, 18-55mm f/3.5-5.6) shooting in RAW format mounted on a tripod was used to capture approximately 36 photographs of each rock (Fig. 3). Approximately 12 photographs were taken while rotating the rock 30° clockwise between shots. The rock was then flipped over and the process was repeated as many times as necessary to photograph every surface of the rock from multiple angles.

An image converter program (CR2 Converter; www.cr2converter.com) was used to convert the file type of the photographs from RAW to PNG to enable easier post-processing. The background of every photograph was cropped using Adobe Photoshop© (Creative Suite 5.5, Adobe Systems, San Jose, California) so that only the image of the rocks remained. The cropped photos were then used to render a three-dimensional (3-D) model of each rock using PhotoScan (version 1.1.6, Agisoft, St. Petersburg, Russia). The models were imported into Meshlab version 1.3.3 (Cignoni, 2014) to calculate volumes and surface areas. Subsequently, a Java program (OBJ Viewer; http://people.eecs.ku.edu/~miller) was used to extract RGB and XYZ data from every vertex on each rock model. The rock models were digitally sliced along the embedding plane (marked in the field) to separate data into ventral and dorsal sides (Fig. 4).

Statistical Analysis

In order to measure melanization (L*) and rubification (a*) on a perceptually uniform scale, the RGB data from the rock vertices were converted into the CIELAB color space following equations given in the software EasyRGB (Logicol S.R.L., Trieste, Italy). Briefly,

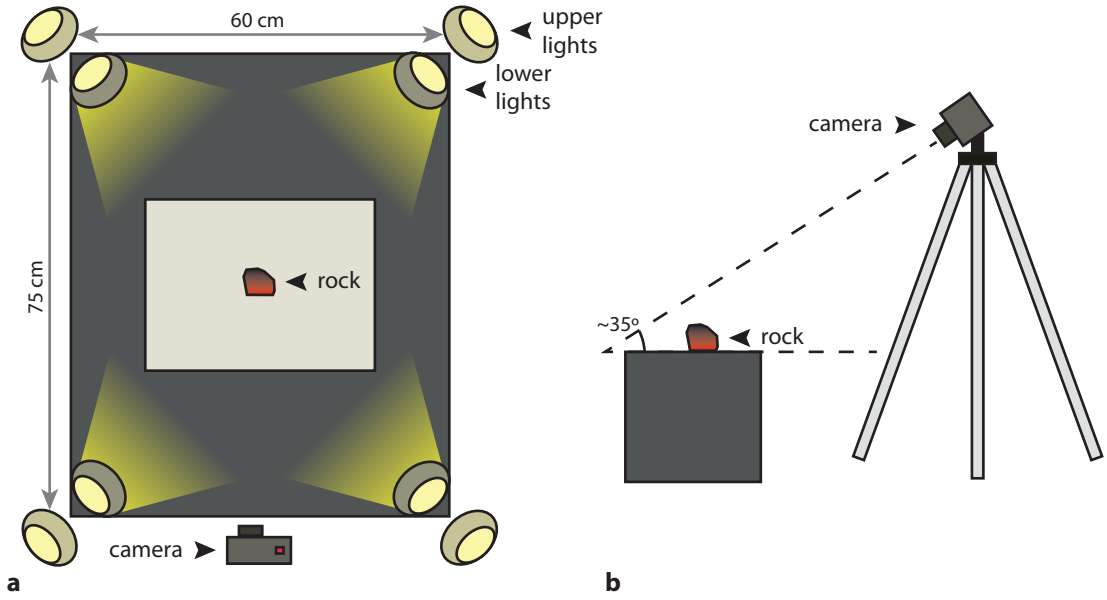

Fig. 3. (a) Plan view of 23-W natural-light fluorescent flood lamps that were positioned around rocks in the laboratory to ensure consistent lighting conditions and minimize shadows when photographing. (b) Profile view of the angle between the rocks and the camera. An additional light (not shown) was positioned just over the camera in (a).

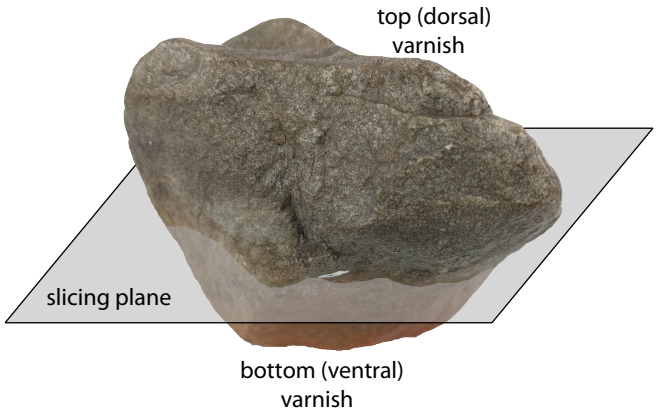

Fig. 4. After rendering, each 3-D model was digitally sliced along the approximate embedding plane to seperate the rubified (bottom) and melanized (top) portions of the rock for further analysis.

color coordinates in the RGB color space, $C_i = \{R, G, B\}$, with the restriction, $0 \leq C_i \leq 255$, were first converted to XYZ color values ($Q_i = \{X, Y, Z\}$) following Eq. (1):

$$Q_i = \begin{cases} q_i^{1/3} & : \quad q_i > 0.008856 \\ 7.877 q_i + 0.1379 & : \quad q_i \leq 0.008856 \end{cases} \tag{1}$$

where $q_i = \{x, y, z\}$ was determined using the following equations:

$$x = 0.4124r + 0.3576g + 0.1805b \tag{2}$$

$$y = 0.2126r + 0.7152g + 0.0722b \tag{3}$$

$$z = 0.0193r + 0.1192g + 0.9505b \tag{4}$$

$$c_i = \begin{cases} 100 \left(\frac{C_i/255 + 0.055}{1.055}\right)^{2.4} & : \quad C_i/255 > 0.04045 \\ C_i/3294.6 & : \quad C_i/255 \leq 0.04045 \end{cases} \tag{5}$$

where $c_i = \{r, g, b\}$. Finally, XYZ values were converted to L*a*b* as follows:

$$L^* = 116Y - 16 \tag{6}$$

$$a^* = 500(X - Y) \tag{7}$$

$$b^* = 200(Y - Z) \tag{8}$$

Volumes, V, were determined from the digital model of each rock and converted to equivalent diameter assuming a spherical shape following Eq. (9):

$$d = 2\left(\frac{3V}{4\pi}\right)^{1/3} \tag{9}$$

Moran's I was applied to assess spatial autocorrelation in the varnish color patterns. Moran's I was calculated following Eq. (10) (Moran, 1950; Brunsdon and Comber, 2015):

$$I = \frac{n}{\sum_i \sum_j w_{ij}} \cdot \frac{\sum_i \sum_j w_{ij}(z_i - \bar{z})(z_j - \bar{z})}{\sum_i (z_i - \bar{z})^2} \tag{10}$$

where n is the number of observations, w_{ij} is the i^{th} and j^{th} element, respectively, of a weights matrix, $\boldsymbol{W}$, that specifies the degree of dependency between the values at location i and j.

Using the R statistical software package (R Core Team, 2016), we analyzed the relationship between L*a*b* components and rock diameter for both volcanic and alluvial rocks. A digital 1 x 1 mm grid was overlaid on the dorsal side of each rock, and the fine-scale roughness of the rock was calculated as the standard deviation of elevation of points falling within each grid cell. This procedure was repeated on the ventral surface of each rock. Similarly, the average L*a*b* values for each grid cell were found. We generated Spearman correlation coefficient histograms to examine the association between rock roughness and both melanization and rubification.

CHAPTER 3. RESULTS AND DISCUSSION

Rock Size Control on Varnish Development

Figure 5a shows the mean L* value for the dorsal side of each rock as a function of rock diameter for both alluvial and volcanic rocks. For reference, low L* values correspond to darker (i.e., more melanized) colors. A clear negative and significant ($P < 0.001$) relationship between rock diameter and L* was observed for the volcanic rocks collected in this study—melanization increased as rocks became larger. This relationship took the form:

$$\overline{L^*} = 40.0 - 7.5\log(\mathrm{d}) \quad (11)$$

where d is effective diameter of the rock. When plot on a linear scale (not shown), this relationship suggests that below a L* value of approximately 33 or beyond effective diameters of ~7 cm, little change in melanization of the dorsal varnish occurs with increasing rock size. No significant trend was detected in the dorsal melanization of alluvial rocks as a function of diameter.

Since dorsal varnish is exposed to the atmosphere and manganese-rich clay particles are primarily deposited by wind, the degree of varnish increases with exposure to the atmosphere (Elvidge and Moore, 1979). Thus, a higher degree of melanization is expected the longer a rock has been stable at the land surface. The negative association between rock size and the L* on the dorsal surfaces of volcanic rocks suggests there may be a rough cutoff point in rock diameter: rocks larger than approximately 7 cm become increasingly difficult to overturn, and are, thus, more stable. This could explain why the association between rock size and dorsal melanization decreases beyond this threshold since these rocks are all relatively likely to remain in place. However, since all sites used in this study lacked significant slopes, the threshold rock diameter needed to maintain stability may be higher on more sloped surfaces. Varnish often reaches

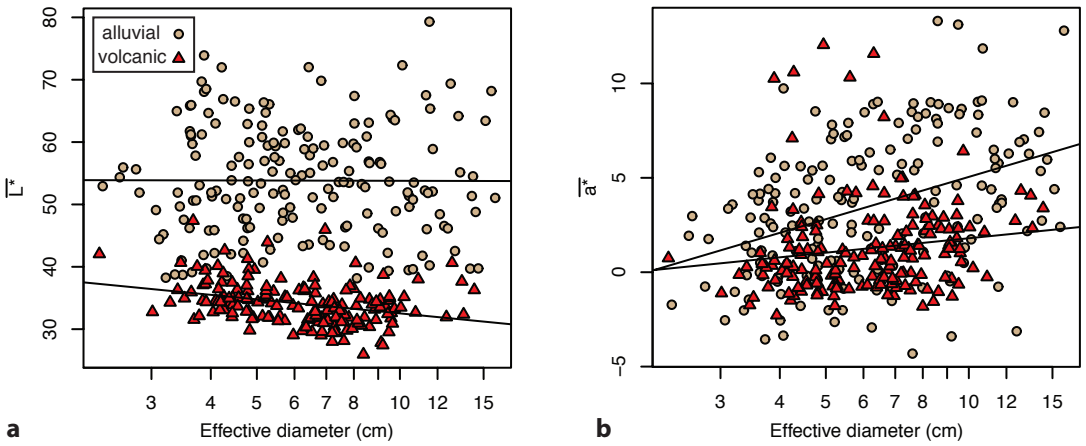

Fig. 5. As rock diameter increases, the (a) dorsal sides of volcanic (red triangles) rocks show significant ($P < 0.001$) melanization while both volcanic ($P = 0.49$) and alluvial (tan circles; $P < 0.001$) rocks show significant rubification on the (b) ventral sides of the rocks.

maximum development on porous rock surfaces, which may explain the lack of a similar relationship with alluvial rocks (Dorn and Oberlander, 1981).

Rubification (increase in a*) on ventral surfaces significantly increased ($P < 0.001$) for both rock types with increasing rock diameter; alluvial rocks showed a steeper positive relationship compared to volcanic rocks (Fig. 5b). The relationship of alluvial and volcanic rock diameter to a* can be described, respectively, as:

$$\overline{a^*} = -2.396 + 7.445\log(\mathrm{d}) \quad (12)$$

$$\overline{a^*} = -0.7398 + 2.5379\log(\mathrm{d}) \quad (13)$$

This shows that, for the rocks studied, ventral rubification appears to be more sensitive to rock diameter than dorsal melanization.

The greater response of ventral rubification may be related to the more protected nature of the buried portion of the rock, which is not subjected to surface weathering, such as sand blasting (Helms et al., 2003). In addition, the ventral sides of rocks accumulate weathered minerals during periodic wetting events (Dorn et al., 2013). Since varnish typically forms at rates of micrometers per millennia, the increased stability of the large diameter rocks would ensure that the ventral side of the rocks stay buried for longer creating an environment conducive to the development of stronger ventral varnish compared to smaller rocks (Dorn, 1998; Liu and Broecker, 2000).

Figure 6a shows the Moran's *I* coefficient of L* values (I_{L*}) for the dorsal side of each rock as a function of rock diameter for both alluvial and volcanic rocks. Moran's *I* indicates the degree of clustering; higher values represent fewer but larger clustered areas of dorsal melanization. A positive and significant ($P < 0.001$) relationship between rock diameter and I_{L*}

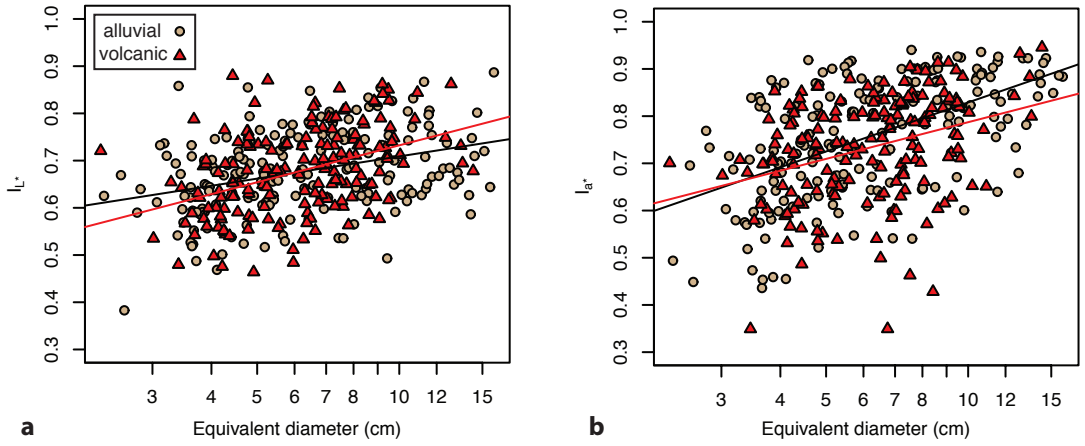

Fig. 6. With larger rock diameters, both (a) melanization on dorsal sides and (b) rubification on the ventral sides of rocks become increasingly clustered as Moran's *I* coefficient approaches +1 ($P < 0.001$). Red triangles refer to volcanic rocks while tan circles correspond to alluvial rocks.

was observed for both volcanic and alluvial rocks showing that larger rocks tended to be associated with more clustered varnish patterns.

The clustering of melanized surfaces on larger diameter rocks suggests that larger rock surface areas are more conducive to varnish formation. Previous studies have pointed to the case hardening effect, in which the cementing agents present in the varnish enhance rock surface resistance to erosion (Dorn, 2004; Aulinas et al., 2014). This differential weathering may encourage additional melanization adjacent to previously established varnished areas while portions of the rock surface lacking adjacent varnish may erode too quickly for new sections of the varnish to form (Conca and Rossman, 1982; Dorn, 2004; Dorn et al., 2012). The increased stability afforded by a larger rock size would encourage the same rock faces to be exposed to the atmosphere for longer periods of time. This would result in more clustered melanization when compared to smaller rocks, which are more easily overturned. More frequent overturning of rocks would result in less consistent and patchy varnish caused by alternating exposed and buried periods.

Figure 6b shows the Moran's *I* coefficient of a* values (I_{a*}) for the ventral side of each rock as a function of rock diameter for both alluvial and volcanic rocks. In this case, as I_{a*} approaches +1, there are fewer but larger areas of rubification on the ventral sides of rocks. As with dorsal surfaces, a similar positive ($P < 0.001$) relationship between rock diameter and I_{a*} was observed on the ventral surfaces for both volcanic and alluvial rocks.

The lowest point of the rocks studied often displayed the most developed rubification. In these cases, iron is likely translocated during wetting events by infiltrating waters to the bottom of the surface rocks. Other rocks displayed the greatest rubification along bands at varying depths under the surface, but not necessarily at the deepest point of the rock. The average depth

of wetting may be influenced by the depth of vesicular horizons—which were present at most of the studied sites—where moisture may be hung up due to matric potential forces imposed by the increase in wind-blown fines in these horizons (Meadows et al., 2008). Additionally, the age of the land surface and the degree of desert pavement formation may reduce infiltration in the vesicular horizon (Young et al., 2004), impacting the depth at which soluble iron is translocated to deeper portions of the rock surface.

Carbonate is known to accumulate as coats underneath rocks after evaporation of percolating waters, with rock size controlling the thickness of these coats through its effect on the presence of macropores (Treadwell-Steitz and McFadden, 2000). As this process furthers, carbonate pendants can form underneath these rocks, although the development of these pendants are complex and depend on the location of voids near the rock surface (Brock and Buck, 2005). This process may nonetheless serve as an analog for the process of iron translocation in the development of ventral rubification. Daily wetting and drying cycles can dissolve and oxidize mineral species deposited on rocks by aeolian processes leaving behind an iron precipitate (Perry and Kolb, 2004).

Roughness-Varnish Expression Relationships

Figure 7 shows the Spearman correlation coefficients between L* and dorsal rock surface roughness. These coefficients were calculated on each rock by correlating surface roughness at pixel sizes of 1 mm to their melanization values. A correlation of +1 indicates a perfect positive relationship between L* and roughness and a correlation of -1 indicates a perfect negative relationship. After determining these correlation coefficients, the rocks were split between alluvial and volcanic and then further subdivided into small, medium, and large size classes as

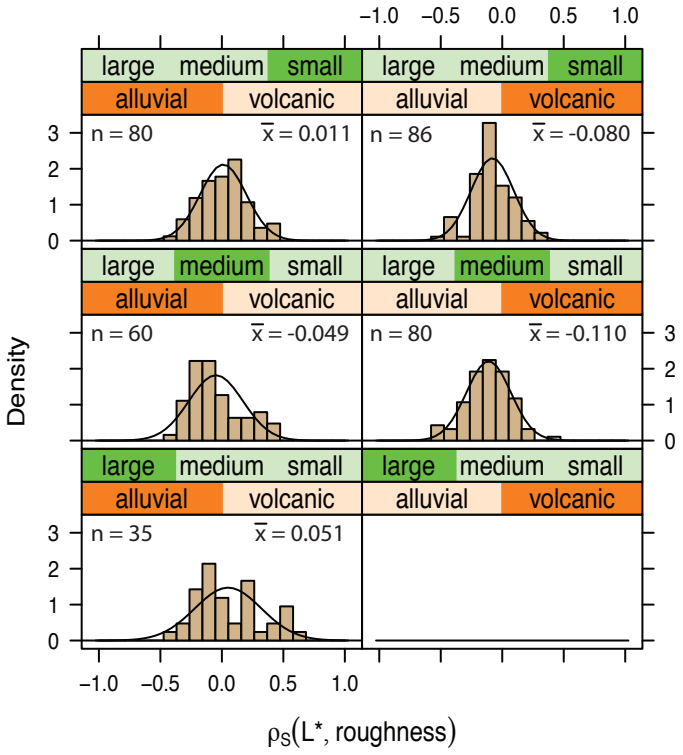

Fig. 7. Histograms of Spearman correlation coefficients calculated to express the association between L* and surface roughness on the dorsal surface of each rock used in this study. Alluvial rocks are shown on the left side of the plot and volcanic rocks are shown on the right side. Rock size class increases from top to bottom. Large volcanic rocks were not observed at the sites studied.

presented in Fig. 7. Higher intensities of dorsal melanization as a function of roughness are shown by increasingly negative Spearman values. This plot shows a slight shift toward more negative values as volcanic rocks increase in size while alluvial rocks show no significant change or difference from a mean of zero ($P > 0.05$).

Since manganese deposition is mainly aeolian, the ability for rocks to capture fines during deposition events may largely determine the extent to which the dorsal sides of the rocks are melanized (Aulinas et al., 2015). There may be a roughness threshold over which rocks are able to encourage the deposition of manganese to produce noticeable melanization. When the rock surface is smooth (e.g., alluvial rocks), dorsal melanization may be retarded due to a lack of manganese deposition.

Figure 8 displays Spearman correlation coefficients between a* and ventral rock surface roughness. Higher correlation values indicate positive relationships between a* and roughness. Lower intensities of ventral rubification as a function of increasing roughness is shown by increasingly negative Spearman values for increasing rock size. This plot shows a sizable shift toward more negative values as alluvial rock size increases; smoother rocks show higher degrees of rubification, especially in the medium and large size classes. The relationship between roughness and rubification does not appear to be impacted by size on volcanic rocks.

A smooth ventral surface appears to be a key factor in determining the strength and extent of ventral rubification. After wetting events, soluble iron is translocated along the edge of the buried rock surface to the deepest point of the rock or shallower depending on the depth and extent of any vesicular horizon (Perry and Kolb, 2004). Since mineral precipitation occurs near the contact between the rock and soil, a smoother surface would put more of the ventral sides of rocks into contact with precipitating iron rather than one with many isolated crevices. The

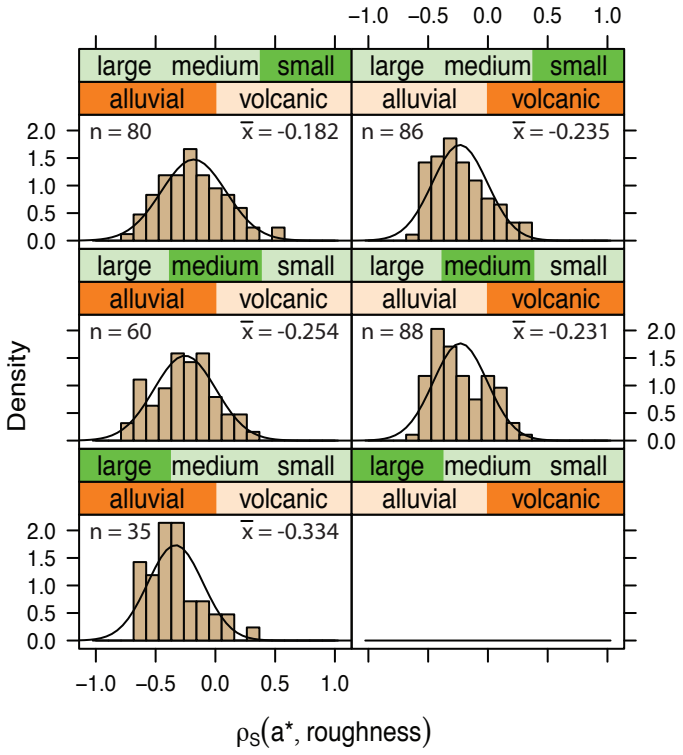

Fig. 8. Histograms of Spearman correlation coefficients calculated to express the association between a* and surface roughness on the ventral surface of each rock used in this study. Alluvial rocks are shown on the left side of the plot and volcanic rocks are shown on the right side. Rock size class increases from top to bottom. Large volcanic rocks were not observed at the sites studied.

longer a consistent environment is maintained (the ventral surface remains at a constant depth), the more rubification can be expressed, as shown by the more stable larger rocks displaying increasingly stronger expressions of varnish.

Landform Varnish Development Through Time

Figure 9 shows the ratio of ventral a* values to dorsal L* values plot against an index developed by Turk and Graham (2011) that describes the degree of V horizon expression. The mean L* value of all pixels on the dorsal sides of individual rocks was calculated and the mean a* value was calculated from the ventral sides of individual rocks. The mean ventral a* value was divided by the mean dorsal L* value from each study area to produce this ratio. A higher ratio indicates more highly developed varnish since an increase in a* on ventral surfaces (numerator) shows stronger rubification while a decrease in L* on dorsal surfaces (denominator) shows stronger melanization. This index is compared to the sum of the quantity of vesicular pores and the size of vesicular pores as described in the field, two factors indicating more well developed vesicular horizons. This plot shows a positive trend between increasing vesicular horizon development and overall varnish intensity.

Using a chronosequence of alluvial fans in the Mojave Desert, Turk and Graham (2011) showed that site age corresponded well with their index of V horizon expression ($R^2 = 0.94$). Properties of V horizons are known to change with age where older horizons are associated with an increase in silt and clay particles (Meadows et al., 2008). This increase suggests that moisture from wetting events on older landscapes may be retained longer in the V horizon.

Figure 10a sets the ratio between ventral rubification and dorsal melanization of rock surfaces described in Fig. 9 against the age of the sites used in this study determined in previous

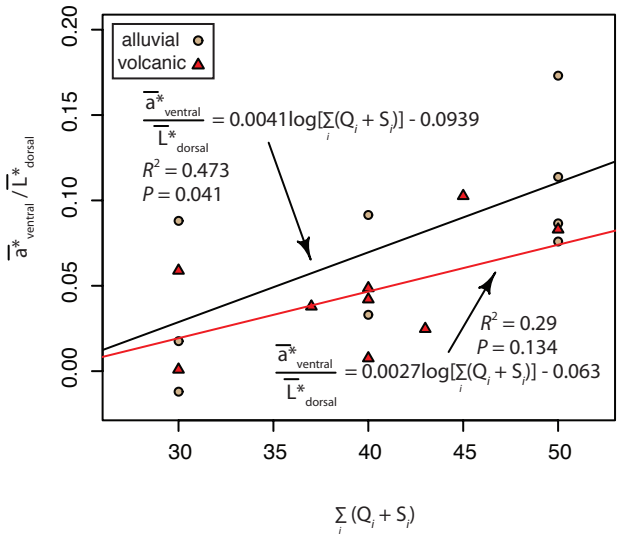

Fig. 9. Degree of varnish expression quantified using the ratio of the a*-value on the ventral surface of the rock to the L*-value on the dorsal surface plotted against an index developed by Turk and Graham (2011) where S_i is size class and Q_i is quantity class of the *i*th vesicular pore described in the V horizon.

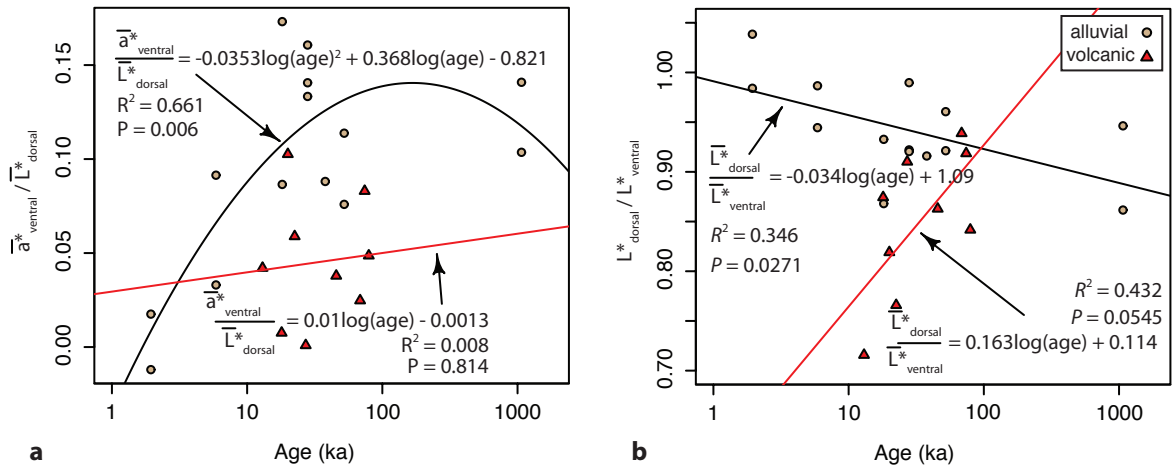

Fig. 10. Varnish development quantified by two indices on large and medium alluvial and volcanic rocks plotted against site age. Red triangles refer to volcanic rocks while tan circles correspond to alluvial rocks.

investigations (Table 1). An overall positive relationship between varnish development and age can be seen for both volcanic rocks and alluvial rocks. We used a quadratic equation to fit alluvial data because it followed the shape of the data more closely. For the quadratic model, age explained 66.1% of the variance in varnish intensity on alluvial rocks ($P < 0.01$), while a linear relationship applied to volcanic rocks did not show a significant relationship ($P = 0.814$).

Varnish development for alluvial rocks increased with site age until around 20 ka (Fig. 10a). In a study by Meadows et al. (2008), soils at sites younger than ~10 ka showed higher rates of infiltration which gradually decreased as the ~10 ka threshold was approached. After ~10 ka, the decrease in infiltration with age was insignificant. This suggests a threshold after which age would have little impact on the rate of varnish formation. The darker base color of volcanic rocks may explain why no significant relationship between varnish development and age was found. In the future, we recommend normalizing the exterior varnish color with the interior color of the rock to overcome this effect.

Figure 10b sets the ratio between dorsal melanization and ventral melanization of rock surfaces against the age of the sites used in this study. A positive relationship between varnish development and age can be seen for volcanic rocks; however, alluvial rocks exhibit a negative relationship that is significant ($P = 0.027$).

A negative relationship is expected because the index for this plot sets the L* of dorsal surfaces over the L* of ventral surfaces and dorsal melanization would decrease the L* of the numerator while ventral rubification would increase the L* of the denominator. Since the L* is being measured for ventral surfaces, the lightening effect of rubification may not be as apparent if a* were being measured, especially on volcanic rocks. Additionally, the narrower range of ages for volcanic rocks makes the positive trend observed for these rocks suspect.

CHAPTER 4. CONCLUSIONS

The goal of this work was to relate varnish expression to known surface ages at a variety of dated sites throughout the Mojave Desert. Diameter proved to be a key component in determining the stability of rocks as larger rocks are more difficult to overturn and, thus, better represent the ages of the landforms in which they are imbedded. Since manganese deposition (melanization) requires an exposed rock surface and iron deposition (rubification) requires a buried rock surface, the longer a rock can maintain its orientation relative to the surface, the more likely a varnish will develop and become strongly expressed. In addition, larger rocks allow varnish to form in clustered areas on the rock surface. This was especially noticable on the smooth undersides of alluvial rocks.

Fine-scale roughness was an important property for the development of ventral varnish on alluvial rocks. Smoother rock surfaces appeared to allow more consistent contact with precipitating iron when moisture from periodic wetting events infiltrates along the rock surfaces and concentrates on the lowest, most deeply embedded portions of the rocks. While the ventral sides of alluvial rocks showed an increasing relationship between a* value and roughness with increasing size class, size had no significant impact on this relationship for volcanic rocks.

The presence of vesicular horizons limits infiltration and concentrates water and solutes at shallower depths where they act to form a ventral varnish. The degree of varnish expression for alluvial rocks corresponded with age until a threshold of around 20 ka after which infiltration rates stabilized. The interplay between rock stability and vesicular horizon development is key to understanding the link between landform age and varnish expression, especially ventral varnish. Larger rocks are more likely to provide a stable embedding plane and, thus, a more consistent environment for varnish formation. In the absence of V horizons, the lowest point of

the ventral surface appears to interact the most strongly with precipitating iron. Where there are vesicular horizons, they can cause the most strongly developed varnish to form at the depths where they are present. This study shows that quantified varnish color may be used be as a proxy for land surface age and stability in the absence of absolute dating techniques on desert pavement-mantled surfaces of the Mojave Desert.

REFERENCES

Aulinas, M., Garcia-Valles, M., Fernando-Turiel, J. L., Gimeno, D., Saavedra, J., Gisbert, G., 2015. Insights into the formation of rock varnish in prevailing dusty regions. Earth Surfaces Processes and Landforms 40, 447-458.

Beck, W., Donahue, D. J., Jull, A. J. T., Burr, G., 1998. Ambiguities in direct dating of rock surfaces using radiocarbon measurements. Science 280, 2132-2135.

Bedford, D. R., Miller, D. M., Phelps, G. A., 2006. Preliminary Surficial Geologic Map of the Amboy 30x60 Minute Quadrangle, California. United States Geological Survey.

Birkeland, P. W., 1984. Soils and Geomorphology. Oxford University Press, New York.

Brock, A. L., Buck, B. J., 2005. Polygenetic development of the Mormon Mesa, NV petrocalcic horizons: Geomorphic and paleoenvironmental interpretations. Catena 77, 65-75.

Brundson, C., Comber, L., 2015. An Introduction to R for Spatial Analysis and Mapping. Sage, Thousand Oaks, CA.

Calzia, J. P., Frisken, J. G., Jachens, R. C., McMahon, A. B., Rumsey, C. M., 1987. Mineral resources of the Kingston Range Wilderness Study Area, San Bernardino County, California. U.S. Geological Survey Bulletin 1709-D.

Conca, J., Rossman, G. R., 1982. Case hardening of sandstone. Geology 10, 520-523.

Cooke, R. U., Warren, A., Goudie, A., 1993. Desert Geomorphology. UCL Press, Ltd., London, pp. 526.

Dibblee, T. W., 1967. Geologic Map of the Old Woman Springs Quadrangle, San Bernardino County, California. United States Geological Survey.

Dorn, R. I., 1998. Response to: Ambiguities in direct dating of rock surfaces using radiocarbon measurements. Science 280, 2136-2139.

Dorn, R. I., 2004. Case hardening. In: Goudie, A. S. (Ed.), Encyclopedia of Geomorphology. Routledge, pp. 118-119.

Dorn, R. I., 2009a. Desert rock coatings. In: Abrahams, A. D., Parsons, A. J. (Eds.), Geomorphology of Desert Environments. Chapman and Hall, pp. 153-186.

Dorn, R. I., 2009b. Rock varnish and its use to study climate change in geomorphic settings. In: Abrahams, A. D., Parsons, A. J. (Eds.), Geomorphology of Desert Environments. Chapman and Hall, pp. 657-673.

Dorn, R. I., Dorn, J., Harrison, E., Gutbrod, E., Gibson, S., Larson, P., Cerveny, N., Lopat, N., Groom, K. M., Allen, C., 2012. Case hardening vignettes from the western USA: Convergence of form as a result of divergent hardening processes. Association of Pacific Coast Geographers Yearbook 74, 1-12.

Dorn, R. I., Krinsley, D. H., Langworthy, K. A., Ditto, J., Thompson, T. J., 2013. The influence of mineral detritus on rock varnish formation. Aeolian Research 10, 61-76.

Dorn, R. I., Oberlander, T. M., 1981. Microbial origin of rock varnish. Science 213, 1245-1247.

Dorn, R. I., Oberlander, T. M., 1982. Rock varnish. Progress in Physical Geography 6, 317-367.

Elvidge, C. D., Moore, C. B., 1979. A model for desert varnish formation. GSA Abstracts and Programs 11, 271.

Harvey, A. M., Wells, S. G., 2003. Late Quaternary alluvial fan development, relations to climatic change, Soda Mountains, Mojave Desert, California. Geological Society of America Special Paper 368, 207-230.

Helms, J. G., McGill, S. F., Rockwell, T. K., 2003. Calibrated, late Quaternary age indices using clast rubification and soil development on alluvial surfaces in Pilot Knob Valley, Mojave Desert, southeastern California. Quaternary Research 60, 377-393.

Hirmas, D. R., Graham, R. C., 2011. Pedogenesis and soil-geomorphic relationships in an arid mountain range, Mojave Desert, California. Soil Science Society of America Journal 75, 192-206.

Liu, T., 2003. Blind testing of rock varnish microstratigraphy as a chronometric indicator: Results on late Quaternary lava flows in the Mojave Desert, California. Geomorphology 53, 209-234.

Liu, T., 2008. VML Dating Lab, http://www.vmldating.com/ [accessed June 16, 2016].

Liu, T., Broecker, W. S., 2013. Millennial-scale varnish microlamination dating of late Pleistocene geomorphic features in the drylands of western USA. Geomorphology 187, 38-60.

Liu, T. Z., Dorn, R. I., 1996. Understanding the spatial variability of environmental change in drylands with rock varnish microlaminations. Annals of the Association of American Geographers, 86, 187-212.

Mahan, S. A., Miller, D. M., Menges, C. M., Yount, J. C., 2007. Late Quaternary stratigraphy and luminescence geochronology of the northeastern Mojave Desert. Quaternary International 166, 61-78.

Matmon, A., Simhai, O., Amit, R., Haviv, I., Porat, N., McDonald, E., Benedetti, L., Robert F., 2009. Desert pavement-coated surfaces in extreme deserts present the longest-lived landforms on Earth. Geological Society of America Bulletin 121, 688-697.

McDonald, E. V., McFadden, L. D., Wells, S. G., 2003. Regional response to alluvial fans to Pleistocene-Holocene climatic transition, Mojave Desert, California. GSA Special Paper 368, 189-205.

McFadden, L. D., Ritter, J. B., Wells, S. G., 1989. Use of multiparameter relative-age methods for age estimation and correlation of alluvial fan surfaces on a desert piedmont, eastern Mojave Desert, California. Quaternary Research 32, 276-290.

Meadows, D. G., Young, M. H., McDonald, E. V., 2008. Influence of relative surface age on hydraulic properties and infiltration on soils associated with desert pavements. Catena 72, 169-178.

Moran, P. A. P., 1950. Notes on continuous stochastic phenomena. Biometrika 37 (1), 17-23.

Perry, R. S., Adams, J. B., 1978. Desert varnish – evidence for cyclic deposition of manganese. Nature 276, 489-491.

Perry, R. S., Kolb, V. M., 2004. Biological and organic constituents of desert varnish: Review and new hypotheses. In: Hoover, R., Rozanov, A. (Eds.) Proceedings of the Society of Photographic Instrumentation Engineers Vol. 5163, Instruments, Methods, and Missions for Astrobiology VII, pp. 202-217.

Phillips, F. M., 2003. Cosmogenic Cl-36 ages of Quaternary basalt flows in the Mojave Desert, California, USA. Geomorphology 53, 199-208.

Poeson, J., Lavee, H., 1991. Effects of size and incorporation of synthetic mulch on runoff and sediment yield from inter-rills in a laboratory study with simulated rainfall. Soil and Tillage Research 21, 209-223.

Potter, R. M., Rossman, G. R., 1977. Desert varnish – importance of clay minerals. Science 196, 1446-1448.

R Core Team, 2016. R: A language and environment for statistical computing, Ver. 3.3.0. R Foundation for statistical computing. Vienna, Austria.

Saleh, A., 1993. Soil roughness measurement: Chain method. Journal of Soil Water Conservation 48, 527-529.

Schoeneberger, P. J., Wysocki, D. A., Benham, E. C., and Soil Survey Staff, 2012. Field book for describing and sampling soils, Version 3.0. National Resources Conservation Service, National Soil Survey Center, Lincoln, NE.

Treadwell-Steitz, C., McFadden, L. D., 2000. Influence of parent material and grain size on carbonate coatings in gravelly soils, Pale Duro Wash, New Mexico. Geoderma 94, 1-22.

Turk, J. K, Graham, R. C., 2011. Distribution and properties of vesicular horizons in the Western United States. Soil Science Society of America Journal 75, 1449-1461.

Wells, S. G., McFadden, L. D., Poths, J., Olinger, C. T., 1995. Cosmogenic He-3 surface-exposure dating of stone pavements: Implications for landscape evolution in deserts. Geology, 23, 613-616.

Young, M. H., McDonald, E. V., Caldwell, T. G., Benner, S. G., Meadows, D. G., 2004. Hydraulic properties of a desert soil chronosequence in the Mojave Desert, USA. Vadose Zone Journal 3, 956-963.